Supermatrix approach to polarized neutron reflectivity from arbitrary spin structures

A. Rühm
Max-Planck-Institut für Metallforschung, Heisenbergstrasse 1, D-70569 Stuttgart, Germany

B. P. Toperverg
Max-Planck-Institut für Metallforschung, Heisenbergstrasse 1, D-70569 Stuttgart, Germany
and Petersburg Nuclear Physics Institute, Gatchina, St. Petersburg 188350, Russia

H. Dosch
Max-Planck-Institut für Metallforschung, Heisenbergstrasse 1, D-70569 Stuttgart, Germany
and Universität Stuttgart, Institut für Theoretische und Angewandte Physik, D–70550 Stuttgart, Germany
(Received 19 May 1999)

The general equation for polarized neutron reflectivity is derived and presented in an invariant vector form that is independent of the selection of a specific coordinate system. Using this representation the reflectivity may easily and thoroughly be analyzed for arbitrary orientation of the sample, the incident beam polarization, and the direction of polarization analysis. It is shown that the complete information that can be extracted from experimental data by a detailed polarization analysis is given by the following quantities: the two complex eigenvalues of the reflectance matrix and a complex vector defining a direction that coincides with the direction of the magnetizations in a collinear magnetization arrangement, but depends on the momentum transfer in the general noncollinear case. A supermatrix formalism is developed and illustrated that allows us to calculate these parameters for multilayers with arbitrary mutual orientation of the magnetizations in individual layers. Our approach opens an alternative way to a complete and unambiguous characterization of artificial magnetic structures of high complexity. [S0163-1829(99)04443-4]

I. INTRODUCTION

The determination of magnetization profiles in complex magnetic systems has been in the focus of scientific interest for several decades.[1–11] Major efforts have been undertaken to reveal and understand the various types of coupling that govern the magnetic structure of both naturally and artificially grown systems on an atomic scale. As demonstrated by a helical sequence in a Fe/La multilayer,[11] today it seems feasible to control the magnetic structure of multilayers on a microscopic scale by applying external magnetic fields during growth, which opens ways to the production of artificial devices with taylored magnetic properties. Both improving quality and rising complexity of magnetic multilayers are to be expected in the future, and both aspects will result in an increasing demand for improved experimental techniques and theoretical concepts providing detailed and accurate information about the microscopic structure of complex magnetic systems.

Neutron reflectometry, as a simple but powerful technique, has been widely used in the past for the characterization of layered magnetization profiles.[6–16] In principle, a three-dimensional polarization analysis of the reflected beam can provide information even about subtle details of a multilayer structure.[8] The outstanding sensitivity of the method to the vector magnetization profile in a sample is mediated by spin-flip processes. In order to account for spin flip, a quantum-mechanical treatment is required, which renders the interpretation of neutron reflectivity from complex noncollinear spin structures less trivial than for x-rays. Matrix formalisms are well suited for practical application and provide a rigorous dynamical approach.[2,3,9] The multiplication of transfer matrices corresponds to recursion steps in the well-known Parratt formalism,[17] with the difference that the latter does not take into account the spin.

The matrix approaches routinely used so far allow to calculate polarized neutron reflectivity from any given spin structure. General software codes including all the necessary coordinate transformations do in fact exist at a few laboratories. However, in the explicit equations published so far[3,18] restrictions have been imposed on the orientation of the neutron polarization and/or the magnetizations in the multilayer in order to simplify notation. It is one of the merits of our closed supermatrix formalism presented in this paper that it is easily adaptable to any experimental situation: Explicit equations are presented in an invariant vector form rendering coordinate transformations unnecessary. The treatment provides a rigorous formalism that is readily applied to layered systems of arbitrary complexity.

II. THEORY

A. Reflectivity

The total Hamiltonian determining neutron reflectivity from a layered system as illustrated in Fig. 1 may be represented as a sum $\hat{\mathcal{H}}=\Sigma\hat{\mathcal{H}}_m$, where the Hamiltonians $\hat{\mathcal{H}}_m = V_m(z)-\hat{\boldsymbol{\mu}}\mathbf{B}_m(z)$ characterizing the individual layers include a nuclear potential $V_m(z)$ and a magnetic contribution proportional to the magnetic induction $\mathbf{B}_m(z)$ within the mth layer. As we will restrict our considerations to the small angle regime, V_m and $\mathbf{B}_m$ may be approximated by constant

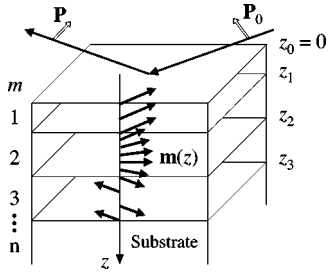

FIG. 1. Sketch of a multilayer with magnetization profile $\mathbf{m}(z)$. In this example one would have to divide layers 2 and 3 further into thinner slabs to obtain constant single-layer magnetizations. The polarizer and analyzer characteristics (direction and efficiency) are represented by $\mathbf{P}_0$ and $\mathbf{P}$.

quantities within each layer. More general profiles can be modeled by further dividing each layer into thin slabs.[17] The magnetic moment of the neutron will be treated as an operator $\hat{\boldsymbol{\mu}}=\mu\hat{\boldsymbol{\sigma}}$, where $\hat{\boldsymbol{\sigma}}=(\hat{\sigma}_x,\hat{\sigma}_y,\hat{\sigma}_z)$ is the vector of Pauli matrices, and the eigenvectors $|\chi\rangle$ of the Hamiltonian $\hat{\mathcal{H}}$ are two-component vectors in the neutron spin space. In the field-free region above the surface ($m=0$) these eigenvectors may be written as

$$|\chi(z)\rangle=\exp(\mathrm{i}p_0z)|t_0\rangle+\exp(-\mathrm{i}p_0z)|r_0\rangle, \tag{1}$$

where $2p_0$ is the wave-number transfer perpendicular to the surface. The first term describes the propagation of the incoming and the second one that of the reflected neutron wave. In the course of reflection the vector $|t_0\rangle$ is transformed into the vector $|r_0\rangle$ by means of the reflectance matrix $\hat{R}$. It is important to realize, however, that it is not the reflectance matrix $\hat{R}$ but only the reflectivity $\mathcal{R}$, which is accessible in an experiment. The latter is given by the mean value of the squared modulus of the matrix element $\langle r|r_0\rangle=\langle r|\hat{R}|t_0\rangle$, where the average is taken with respect to the density matrix of the initial states, $\hat{\rho}_0=\overline{|t_0\rangle\langle t_0|}$, and the one of the final states, $\hat{\rho}=\overline{|r\rangle\langle r|}$. The density matrices are defined by the polarizer and analyzer characteristics. The final result may be represented in the form[2,19]

$$\mathcal{R}=\overline{|\langle r|\hat{R}|t_0\rangle|^2}=\mathrm{Tr}\{\hat{\rho}\hat{R}\hat{\rho}_0\hat{R}^+\}. \tag{2}$$

It is evident from Eq. (2) that the reflectivity $\mathcal{R}$ is influenced by two fundamentally different kinds of quantities, the reflectance matrix characterizing the sample and the density matrices characterizing the specific polarizer-analyzer configuration. However, Eq. (2) does not specify the dependence of $\mathcal{R}$ on the polarization directions and the sample orientation explicitly, which would facilitate its application to experiments. Therefore we will derive a more explicit expression for $\mathcal{R}$ in the following. In order to avoid a complicated notation we will use a vector representation of all the quantities involved in Eq. (2) that contains the vector of Pauli matrices $\hat{\boldsymbol{\sigma}}$. As a major benefit of this procedure, the final result will be invariant under coordinate transformations, in contrast to former approaches to that problem.

To start with, one has to note that the reflectance matrix $\hat{R}$, as any (2×2) matrix, can be decomposed into a sum of two terms according to[19,20]

$$\hat{R}=\tfrac{1}{2}(R_0+\mathbf{R}\hat{\boldsymbol{\sigma}}), \tag{3}$$

where $R_0=\mathrm{Tr}\{\hat{R}\}$ and $\mathbf{R}=\mathrm{Tr}\{\hat{R}\hat{\boldsymbol{\sigma}}\}$. The latter quantities may also be written in the form $R_0=R_++R_-$ and $\mathbf{R}=(R_+-R_-)\mathbf{b}_\mathrm{r}$ with $R_\pm$ denoting the (complex) eigenvalues of the reflectance matrix and $\mathbf{b}_\mathrm{r}\in\mathbb{C}^3$ with $\mathbf{b}_\mathrm{r}^2=1$. By means of Eq. (3) the four (complex) elements of the matrix $\hat{R}$ are parameterized by a complex number R_0 and a complex three-component vector $\mathbf{R}$. The quantities R_0 and $\mathbf{R}$ depend only on the nuclear and magnetic structure of the multilayer, the critical wave numbers, and the wave-number transfer $2p_0$, but not on the polarization of the neutron beams. They are readily derived from the reflectance matrix $\hat{R}$ after the latter has been calculated within the framework of a conventional matrix formalism[3] or, preferably, the supermatrix formalism outlined in Sec. II B below. It is worthwhile to mention that, when the sample is rotated around its surface normal, the vector $\mathbf{R}$ transforms as a normal vector, exactly like the single-layer magnetizations fixed to the sample.

The density matrices in Eq. (2) may be represented in a form very similar to Eq. (3), namely[1,2,19,20]

$$\hat{\rho}_0=\tfrac{1}{2}(1+\mathbf{P}_0\hat{\boldsymbol{\sigma}}) \quad\text{and}\quad \hat{\rho}=\tfrac{1}{2}(1+\mathbf{P}\hat{\boldsymbol{\sigma}}) \tag{4}$$

with $\mathbf{P}_0=P_0\mathbf{n}_0$ and $\mathbf{P}=P\mathbf{n}$, where $\mathbf{n}_0$ and $\mathbf{n}$ are unit vectors in the directions of the initial polarization and the polarization analysis, and P_0 and P are the polarization efficiencies of the polarizing and analyzing device, respectively.

Inserting Eqs. (3) and (4) into Eq. (2) and utilizing the relation $(\mathbf{a}\hat{\boldsymbol{\sigma}})(\mathbf{b}\hat{\boldsymbol{\sigma}})=(\mathbf{ab})+\mathrm{i}(\mathbf{a}\times\mathbf{b})\hat{\boldsymbol{\sigma}}$ for $\mathbf{a},\mathbf{b}\in\mathbb{C}^3$ leads to the final result

$$\begin{aligned}\mathcal{R}=&\tfrac{1}{8}\{|R_0|^2[1+(\mathbf{P}_0\mathbf{P})]+|\mathbf{R}|^2[1-(\mathbf{P}_0\mathbf{P})]\}\\&+\tfrac{1}{4}\mathrm{Re}\{R_0^*\mathbf{R}(\mathbf{P}_0+\mathbf{P})+(\mathbf{R}^*\mathbf{P}_0)(\mathbf{RP})\}\\&-\tfrac{1}{4}\mathrm{Im}\left\{R_0^*\mathbf{R}(\mathbf{P}_0\times\mathbf{P})+\frac{1}{2}(\mathbf{R}^*\times\mathbf{R})(\mathbf{P}_0-\mathbf{P})\right\}.\end{aligned} \tag{5}$$

Although this equation looks complicated at first sight, it boils down to very simple expressions of practical use when it is applied to typical experimental situations. We will illustrate that in Sec. III. At this place, however, we would like to point out that the basic Eq. (5) describes, for any experimental arrangement, the (measurable) neutron reflectivity from a multilayer whose reflectance matrix $\hat{R}$ is connected with R_0 and $\mathbf{R}$ according to Eq. (3). It should also be emphasized, that Eq. (5) represents the reflectivity in an invariant vector form, thereby avoiding the limitations of other theoretical approaches using an explicit notation in a certain coordinate system.[3,9,10,18] A very similar general formula may be derived for grazing-angle neutron diffraction as briefly outlined in Ref. 21.

B. Reflectance matrix

Applying Eq. (5) to practical cases requires the calculation of the reflectance matrix $\hat{R}$ from which R_0 and $\mathbf{R}$ are derived. For that purpose we use a supermatrix formalism with transfer supermatrices $\hat{S}_m$ that transform the neutron

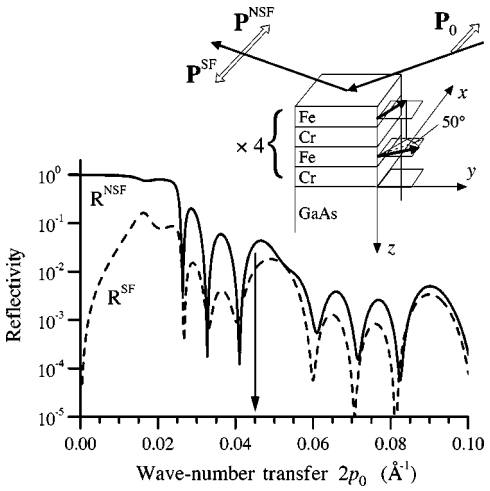

FIG. 2. Calculated non-spin-flip and spin-flip reflectivity for a FeCr multilayer and an experimental setup as depicted in the inset. The multilayer is made up of four identical blocks of two FeCr bilayers each. The incident beam was assumed to be fully polarized along the x axis. The critical wave numbers were $q_{c+}^{\mathrm{Fe}}=0.0128$ Å^{-1}, $q_{c-}^{\mathrm{Fe}}=0.0061$ Å^{-1} (corresponding to magnetically saturated Fe layers) and $q_{\mathrm{c}}^{\mathrm{Cr}}=q_{\mathrm{c}}^{\mathrm{GaAs}}=0.0062$ Å^{-1}. The thickness of the Fe layers was set to 53 Å and that of the Cr layers to 17 Å. The magnetizations in adjacent Fe layers embrace an angle of 50°, which produces a super-structure maximum at the half-order peak position $2p_0=0.045$ Å^{-1} in both reflectivity curves. The slight shift of these maxima against the nominal position marked by the arrow is due to refraction.

wave function $|\chi(z)\rangle$ and its derivative $|\chi'(z)\rangle$, both evaluated at the position $z=z_{m-1}$ of the inner boundary of layer $m-1$ (see Fig. 2), into the corresponding quantities of layer m according to[22]

$$\begin{pmatrix} |\chi(z_m)\rangle \\ |\chi'(z_m)\rangle \end{pmatrix} = \hat{S}_m \begin{pmatrix} |\chi(z_{m-1})\rangle \\ |\chi'(z_{m-1})\rangle \end{pmatrix}. \tag{6}$$

Owing to the continuity conditions at each interface between adjacent layers, the transfer supermatrices are explicitly given by[22–24]

$$\hat{S}_m = \begin{pmatrix} \hat{S}_m^{11} & \hat{S}_m^{12} \\ \hat{S}_m^{21} & \hat{S}_m^{22} \end{pmatrix} = \begin{pmatrix} \cos \hat{p}_m d_m & \hat{p}_m^{-1} \sin \hat{p}_m d_m \\ -\hat{p}_m \sin \hat{p}_m d_m & \cos \hat{p}_m d_m \end{pmatrix}. \tag{7}$$

In this equation, d_m is the thickness of the mth layer and $\hat{p}_m=\{p_0^2-\hat{q}_{mc}^2\}^{1/2}$, where $\hat{q}_{mc}^2=2m/\hbar^2\cdot\hat{\mathcal{H}}_m$. Instead of writing down the four (2×2) elements of the supermatrix $\hat{S}_m$ explicitly, we use again the Pauli matrix representation[19,20]

$$\hat{S}_m^{\mu\nu}=\tfrac{1}{2}\{[S_{m+}^{\mu\nu}+S_{m-}^{\mu\nu}]+(\mathbf{B}_m^0\hat{\boldsymbol{\sigma}})[S_{m+}^{\mu\nu}-S_{m-}^{\mu\nu}]\}, \tag{8}$$

where $\mathbf{B}_m^0=\mathbf{B}_m/|\mathbf{B}_m|$ is a unit vector directed along the magnetic field $\mathbf{B}_m$ in the mth layer and $S_{m\pm}^{\mu\nu}$ are the eigenvalues of the matrices $\hat{S}_m^{\mu\nu}$, e.g., $S_{m\pm}^{11}=\cos p_{m\pm}d_m$, with $p_{m\pm}=\{p_0^2-q_{mc\pm}^2\}^{1/2}$ and $q_{mc\pm}$ denoting the critical wave numbers of total reflection for neutrons with spin parallel and antiparallel to $\mathbf{B}_m$. Due to the invariant form of Eq. (5) any convenient coordinate system may be used to define the components of B_m for numerical calculations.

The final step is to derive the reflectance matrix $\hat{R}$ from the transfer supermatrix $\hat{S}_{\mathrm{tot}}$ that transforms the neutron wave function at the sample surface into the wave function at the semi-infinite substrate (layer $n+1$), that is

$$\begin{pmatrix} |\chi(z_n)\rangle \\ |\chi'(z_n)\rangle \end{pmatrix} = \hat{S}_{\mathrm{tot}} \begin{pmatrix} |\chi(0)\rangle \\ |\chi'(0)\rangle \end{pmatrix} \tag{9}$$

with the four (2×2) elements of $\hat{S}_{\mathrm{tot}}$ given by $\hat{S}_{\mathrm{tot}}^{\mu\nu}=\Sigma_{\lambda,\eta,\ldots,\zeta=1}^{2}\hat{S}_n^{\mu\lambda}\hat{S}_{n-1}^{\lambda\eta}\ldots\hat{S}_1^{\zeta\nu}$, where $\mu,\nu\in\{1,2\}$. It can be seen from Eq. (1) that $|\chi(0)\rangle=(1+\hat{R})|t_0\rangle$ and $|\chi'(0)\rangle=\mathrm{i}p_0(1-\hat{R})|t_0\rangle$. Correspondingly $|\chi(z_n)\rangle=\hat{T}|t_0\rangle$ and $|\chi'(z_n)\rangle=\mathrm{i}p_s\hat{T}|t_0\rangle$, where $\hat{T}$ is the transmittance matrix. After inserting these quantities into Eq. (9) and eliminating $\hat{T}$ one immediately obtains

$$\hat{R}=\hat{\Delta}^{-1}\cdot\{(\hat{S}_{\mathrm{tot}}^{22}-\mathrm{i}p_0^{-1}\hat{S}_{\mathrm{tot}}^{21})p_0-(\hat{S}_{\mathrm{tot}}^{11}+\mathrm{i}p_0\hat{S}_{\mathrm{tot}}^{12})p_s\} \tag{10}$$

with $\hat{\Delta}=(\hat{S}_{\mathrm{tot}}^{22}+\mathrm{i}p_0^{-1}\hat{S}_{\mathrm{tot}}^{21})p_0+(\hat{S}_{\mathrm{tot}}^{11}-\mathrm{i}p_0\hat{S}_{\mathrm{tot}}^{12})p_s$ and $p_s=\{p_0^2-q_{sc}^2\}^{1/2}$, where q_{sc} is the critical wave number in the substrate.

Note that Eqs. (7) and (10) transform into equations well known from the theory of electromagnetic waves[24] as soon as the spin-nature of the neutron is ignored by replacing the four (2×2) elements of the transfer supermatrices in Eq. (7) by their scalar counterparts, e.g., $\cos\hat{p}_m d_m$ by $\cos p_m d_m$.

III. DISCUSSION

The supermatrix approach to neutron reflectivity presented in this paper may be regarded as a straightforward extension of the theory of reflection for electromagnetic waves[24] to the case of neutrons. The clear structure of the formalism provides transparency to the physics behind, which is one of its merits. A second merit is that the formalism is very general and immediately applicable to any experimental arrangement, because the notation does not depend on the selection of a specific coordinate system. Third, the formalism is well suited for implementation in a fitting routine like that available from our internet homepage.[25] The numerical simulation of reflectivity data takes typically only a few seconds per parameter set, including the calculation of the eigenvalues of the reflectance matrix, the vector $\mathbf{b}_r$, the total cross section defined by $d\sigma/d\Omega=\mathrm{Tr}\{\hat{R}\rho_0\hat{R}^+\}$ and the polarization vector of the reflected beam.[1,2,19] In addition, our software delivers the non-spin-flip and spin-flip reflectivities typically measured in a polarized neutron reflection experiment.[3,6,8] Finally, for a fixed wave-number transfer $2p_0$ the dependence of the reflectivity on an azimuthal rotation of the sample may be calculated. Interestingly, the latter may provide valuable information on the magnetization profile in the sample as we will discuss in the following.

In a typical polarized neutron reflection experiment one measures the non-spin-flip and spin-flip reflectivities $\mathcal{R}^{\mathrm{NSF}}=\mathcal{R}(\mathbf{P}=\mathbf{P}_0)$ and $\mathcal{R}^{\mathrm{SF}}=\mathcal{R}(\mathbf{P}=-\mathbf{P}_0)$ for certain orientations of $\mathbf{P}_0$. For this typical case Eq. (5) may be simplified to

$$\mathcal{R}^{\mathrm{NSF}} = \tfrac{1}{4}\,|R_0 + R_{||}|^2, \tag{11}$$

$$\mathcal{R}^{\mathrm{SF}} = \tfrac{1}{4}\,(|\mathbf{R}|^2 - |R_{||}|^2) + \tfrac{1}{4}\mathrm{Im}(\mathbf{R}\times\mathbf{R}^*)_{||}, \tag{12}$$

where the suffixes ''||'' denote the projection on $\mathbf{P}_0$, e.g., $R_{||} = \mathbf{R}\mathbf{P}_0$. If we express R_0 and $\mathbf{R}$ in terms of the eigenvalues of the reflectance matrix and the vector $\mathbf{b}_\mathrm{r}$, then Eqs. (11) and (12) may be written as

$$\mathcal{R}^{\mathrm{NSF}} = |(R_+ + R_-) + (R_+ - R_-)\cos\gamma|^2, \tag{13}$$

$$\mathcal{R}^{\mathrm{SF}} = \tfrac{1}{4}\,|R_+ - R_-|^2 \times [|\mathbf{b}_\mathrm{r}|^2 - |\cos\gamma|^2 + \mathrm{Im}(\mathbf{b}_\mathrm{r}\times\mathbf{b}_\mathrm{r}^*)_{||}], \tag{14}$$

where the (complex) angle γ is defined by $\cos\gamma = \mathbf{b}_\mathrm{r}\mathbf{P}_0$. For *collinear* magnetization profiles $\mathbf{b}_\mathrm{r}$ is real valued and coincides with the magnetization direction in the layers. In that case, Eq. (14) may be simplified to

$$\mathcal{R}^{\mathrm{SF}} = \tfrac{1}{4}\,|R_+ - R_-|^2 \sin^2\gamma, \tag{15}$$

and γ is the *real* angle between the magnetization direction in the sample and the polarization vector $\mathbf{P}_0$ of the incident beam.

In the following, we will illustrate and discuss these equations by means of the noncollinear magnetization profile depicted in Fig. 2. The multilayer is made up of eight identical FeCr bilayers deposited on GaAs with zero magnetization in the Cr layers and magnetically saturated Fe layers. Motivated by previous experiments[8] we assumed that the direction of the Fe magnetizations oscillates with a period of two bilayers and the magnetizations in adjacent Fe layers embrace an angle of 50°. The non-spin-flip and spin-flip reflectivity curves in Fig. 2 are calculated according to Eqs. (13) and (14) for an incident beam polarization $\mathbf{P}_0 = \mathbf{x}^0$, where $\mathbf{x}^0$ denotes the unit vector along the *x*-axis.

The example depicted in Fig. 2 is well suited to reveal a fundamental difference between collinear and noncollinear magnetization profiles in regard to polarized neutron reflectometry. A general analysis of Eqs. (13) to (15) shows that the presumption of a collinear magnetization profile seriously reduces the variety of reflectivity data sets that can be modeled. This may be most easily demonstrated by the dependence of the reflectivity on an azimuthal rotation of the sample. This dependence turns out to be qualitatively different for collinear and noncollinear arrangements, respectively, due to the fact that in the general noncollinear case $\mathbf{b}_\mathrm{r}$ and γ are complex quantities.

In the collinear case an azimuthal rotation of the sample around its surface normal would result in a variation of the non-spin-flip intensity $\mathcal{R}^{\mathrm{NSF}}$ with the rotation angle ω that obeys $\mathcal{R}^{\mathrm{NSF}}(\omega) = \mathcal{R}^{\mathrm{NSF}}(-\omega)$ and $\mathcal{R}^{\mathrm{NSF}}(\pi+\omega) = \mathcal{R}^{\mathrm{NSF}}(\pi - \omega)$, if one defines $\omega := 0$ for a situation where the projections of $\mathbf{b}_\mathrm{r}$ and $\mathbf{P}_0$ onto the surface are collinear. Both symmetries are usually broken in case of a noncollinear magnetization structure as evidenced by the example illustrated in Fig. 3. The thin-solid line represents an approximation of $\mathcal{R}^{\mathrm{NSF}}$ that has been calculated under the assumption of a collinear magnetization arrangement according to $\mathcal{R}^{\mathrm{NSF}}_{\mathrm{approx}} = A + B\cos(\omega-\omega_0) + C\cos^2(\omega-\omega_0)$ with $\omega_0, A, B, C \in \mathbb{R}$. This approximation obeys the symmetry relations given above and may be shown to cover the whole set of functions that can be calculated on the basis of Eq. (15).

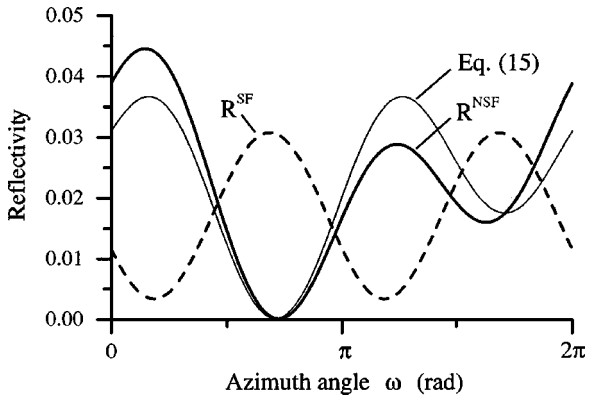

FIG. 3. Variation of the non-spin-flip and spin-flip reflectivity in dependence of the azimuthal rotation angle ω as calculated for the sample and the experimental setup depicted in Fig. 3. The data are calculated for a wave-number transfer $2p_0 = 0.045$ Å^{-1} corresponding to the half-order position marked by the arrow in Fig. 2. The thin-solid line represents another non-spin-flip signal calculated according to Eq. (15) under the assumption of a collinear magnetization profile. In contrast to $\mathcal{R}^{\mathrm{NSF}}$, it obeys the symmetry relations given in the text.

The spin-flip reflectivity $\mathcal{R}^{\mathrm{SF}}$ shows an other characteristic deviation from the behavior expected for a collinear magnetization profile. As shown in Fig. 3, it does not vanish for any value of ω, which is in contradiction to Eq. (15) unless there is a magnetization component perpendicular to the surface. However, frequently this can be ruled out in practice, since the perpendicular component would also be present above the surface due to continuity requirements. As evidenced by Fig. 3, however, in the noncollinear case a perpendicular magnetization component is not required to produce a constant offset in the azimuthal variation of $\mathcal{R}^{SF}$ with ω. This may be explained by the fact that in a noncollinear arrangement not all the Fe magnetizations can be aligned with the polarization of the incident beam simultaneously; therefore, there is always at least one Fe layer causing spin flip.

While the offset in the spin-flip intensity in an azimuthal reflectivity scan might also be caused by a constant background or an imperfect polarizer or analyzer efficiency in a real experiment, the fundamentally altered symmetry of the non-spin-flip intensity may serve as an unambiguous criterion for a noncollinear spin structure in a specific sample. On the basis of our results we suggest to record an azimuthal reflectivity scan in any neutron reflection experiment where a noncollinear spin structure is to be expected in the sample. In contrast to a complete setup for three-dimensional polarization analysis a sample rotation stage may be easily implemented in existing experimental stations. Special measures may be required to examine samples in an external magnetic field rotated together with the sample, since any influence of the field on the neutron beams outside the sample has to be avoided.

IV. SUMMARY

We combined several theoretical concepts developed for the analysis of neutron reflection and diffraction data to an

exact, but still simple, closed matrix formalism that may be directly applied to calculate the measurable reflectivity from multilayer systems of in principle arbitrary complexity. Analogously to the Parratt formalism our supermatrix approach also provides an approximate solution for continuous magnetization profiles. The source code of our simulation software is available from our internet homepage.[25]

Using our formalism, we demonstrated that in polarized neutron reflection experiments an azimuthal sample rotation may provide direct evidence for noncollinear spin structures. The dependence of the reflected intensity on the azimuth angle should be recorded at least at some positions in the reflectivity curve in order to avoid misinterpretation of measured neutron reflectivity data.

ACKNOWLEDGMENTS

We thank O. Schärpf (ILL, Grenoble) for assistance during the software development and J. Major (MPI für Metallforschung, Stuttgart) for helpful discussions. This work was supported by the RFFI under Grant No. L-EN-96-15-96775 and the Russian State Program ''Neutron Research of Condensed Matter.''

[1] M. Blume, Phys. Rev. **130**, 1670 (1963).
[2] S. K. Mendiratta and M. Blume, Phys. Rev. B **14**, 144 (1976).
[3] G. P. Felcher, R. O. Hilleke, R. K. Crawford, J. Haumann, R. Kleb, and G. Ostrowski, Rev. Sci. Instrum. **58**, 609 (1987).
[4] E. E. Fullerton, S. D. Bader, and J. L. Robertson, Phys. Rev. Lett. **77**, 1382 (1996).
[5] R. S. Fishman, Phys. Rev. Lett. **81**, 4979 (1998).
[6] C. F. Majkrzak, Physica B **173**, 75 (1991).
[7] G. P. Felcher, Physica B **192**, 137 (1993).
[8] A. Schreyer, J. F. Ankner, Th. Zeidler, H. Zabel, M. Schäfer, J. A. Wolf, P. Grünberg, and C. F. Majkrzak, Phys. Rev. B **52**, 16 066 (1995).
[9] S. J. Blundell and J. A. C. Bland, Phys. Rev. B **46**, 3391 (1992).
[10] C. F. Majkrzak, Physica B **221**, 342 (1996).
[11] G. P. Felcher, W. Lohstroh, H. Fritzsche, M. Münzenberg, H. Maletta, and W. Felsch, Appl. Phys. Lett. **72**, 2894 (1998).
[12] H. Zabel, Physica B **198**, 156 (1994).
[13] A. Schreyer, J. F. Ankner, H. Zabel, M. Schäfer, C. F. Majkrzak, and P. Grünberg, Physica B **198**, 173 (1994).
[14] F. Klose, Ch. Rehm, D. Nagengast, H. Maletta, and A. Weidinger, Phys. Rev. Lett. **78**, 1150 (1997).
[15] A. Schreyer, C. F. Majkrzak, Th. Zeidler, T. Schmitte, P. Bödeker, K. Theis-Bröhl, A. Abromeit, J. A. Dura, and T. Watanabe, Phys. Rev. Lett. **79**, 4914 (1997).
[16] C. F. Majkrzak, N. F. Berk, J. A. Dura, S. K. Satija, A. Karim, J. Pedulla, and R. D. Deslattes, Physica B **248**, 338 (1998).
[17] L. G. Parratt, Phys. Rev. **95**, 359 (1954).
[18] C. F. Majkrzak, Physica B **156&157**, 619 (1989).
[19] W. Marshall and S. W. Lovesey, *Theory of Thermal Neutron Scattering* (Clarendon Press, Oxford, 1971), pp. 324–331.
[20] L. D. Landau and E. M. Lifshitz, *Quantum Mechanics* (Pergamon Press, Oxford, 1977), pp. 193–196.
[21] B. P. Toperverg, A. Rühm, W. Donner, and H. Dosch, Physica B **246**, 198 (1999).
[22] Note that the order of the elements of the four-component vectors in Eq. (6) is different from the one used in many other publications (e.g., Ref. 3). However, it is essential to use the order presented in this article in order to obtain Eq. (7) and to profit from the simplifications arising from this equation.
[23] P. Croce and B. Pardo, Nouv. Rev. Opt. Appl. **1**, 229 (1970).
[24] M. Born and E. Wolf, *Principles of Optics* (Pergamon Press, Oxford, 1975), pp. 51–70.
[25] Our simulation software is available via the respective links on our internet homepage: http://wwwmf.mpi-stuttgart.mpg.de/abteilungen/dosch/dosch.html